Visualizing high-temperature spin dynamics in $La_{1-x}Ca_xMnO_3$ from a mapping of EPR linewidth and *g*-factor

2007 J. Phys.: Condens. Matter 19 196213

(http://iopscience.iop.org/0953-8984/19/19/196213)

IOP PUBLISHING JOURNAL OF PHYSICS: CONDENSED MATTER

J. Phys.: Condens. Matter **19** (2007) 196213 (12pp) doi:10.1088/0953-8984/19/19/196213

Visualizing high-temperature spin dynamics in $La_{1-x}Ca_xMnO_3$ from a mapping of EPR linewidth and *g*-factor

Y Liu[1,3], **S L Wan**[1] **and X G Li**[2]

[1] Department of Modern Physics, University of Science and Technology of China, Hefei 230026, People's Republic of China
[2] Hefei National Laboratory for Physical Sciences at Microscale, Department of Physics, University of Science and Technology of China, Hefei 230026, People's Republic of China

E-mail: yliu@ustc.edu.cn

Received 5 February 2007, in final form 16 March 2007
Published 19 April 2007
Online at stacks.iop.org/JPhysCM/19/196213

Abstract

We report the measurements of electron paramagnetic resonance (EPR) on powder samples of $La_{1-x}Ca_xMnO_3$ (LCMO) at the commensurate carrier concentrations of $x = N/8$ ($N = 1, 2, 3, 4, 5, 6$, and 7) within the temperature range 100 K $\leqslant T \leqslant$ 450 K. It is found that the mapping of the EPR linewidth ΔH and the g-factor shows an electron–hole asymmetry in the paramagnetic insulating regime of the LCMO phase diagram. The drop of linewidth ΔH with decreasing temperature in the mapping resembles the contour of the ferromagnetic transition curve in the LCMO phase diagram, while the isothermal ΔH becomes narrowest at $x = 3/8$ due to the predominant double exchange interaction. By comparing the small-polaron model with spin–spin relaxation mechanism, we demonstrate that the latter should dominate the paramagnetic insulating regime of the LCMO phase diagram.

(Some figures in this article are in colour only in the electronic version)

1. Introduction

Due to a complex interplay among charge, spin, orbital, and lattice degrees of freedom, $La_{1-x}Ca_xMnO_3$ (LCMO) shows a rich phase diagram as a function of doping, temperature, and magnetic field [1]. It is generally accepted that the competition between the double exchange (DE) interaction [2] and an enhanced electron–phonon coupling via the Jahn–Teller (JT) active Mn^{3+} ion [3] plays a key role in determining the phase diagram of the manganites. A qualitative picture to explain the phase diagram of LCMO suggests that the ferromagnetic metallic (FM) ground state occurs due to the predominant DE mechanism for $x < 0.5$, while a charge ordering

[3] Author to whom any correspondence should be addressed.

(CO) state tends to stabilize with x exceeding 0.5, where the dominant mechanism responsible for the charge order is the JT coupling, with a lesser but significant contribution from the on-site Coulomb interaction [4]. In contrast to rich doping-dependent ground states, the high-temperature paramagnetic insulating (PI) regime above the ordering temperatures seems to be simply dominated by the self-trapped small polarons [3, 5].

Most studies, such as electrical and thermal measurements, suggest that electron–phonon and on-site Coulomb interactions dominate in the high-temperature PI regime, while magnetic correlations could be completely ignored [5]. In fact, this might be the case in a high enough temperature regime. X-ray and neutron scattering measurements have directly demonstrated the presence of short-range polaron correlations in the PI phase of optimally doped manganites [6–8]. The results strongly suggest that magnetic interactions are enhanced when considering short-range polaron correlations with decreasing temperature in the PI regime of the LCMO phase diagram. An analysis of the spin–spin correlations based on Monte Carlo calculations shows that ferromagnetic clusters form with a size of three-to-four lattice spacings above the Curie temperature T_C [9]. One can suppose that the short-range CO correlation is possibly in the form of an FM zigzag structure, a small segment of the CE-type CO state [10]. For the CE-type magnetic structure, an equal number of Mn^{3+} and Mn^{4+} ions show a real space ordering, while the e_g orbitals of Mn^{3+} form zigzag chains in the *ac* plane. The core spins in the zigzag chains are FM coupled by DE interaction [11].

The main purpose of this study is to depict the spin dynamics in the PI regime of the LCMO phase diagram. Electron paramagnetic resonance (EPR) is a powerful probe of spin dynamics in the manganites. We report a systematic investigation of the temperature dependences of the EPR line resonance field (g-factor), linewidth ΔH, and intensity I for polycrystalline samples of LCMO at the commensurate carrier concentrations of $x = N/8$ ($N = 1, 2, 3, 4, 5, 6$, and 7). As is evident in the phase diagram, there are well defined features at the commensurate carrier concentrations of $x = N/8$ ($N = 1, 3, 4, 5$, and 7) in LCMO [1], e.g., optimal doping for the FM state at $x = 3/8$, and the highest CO temperature T_{CO} at $x = 5/8$. Moreover, the Curie temperature T_C is similar to the temperature T_{CO} for the two doping levels, forming an electron–hole symmetry phase line centred at $x = 4/8$.

2. Experimental details

Polycrystalline samples of LCMO with commensurate doping of $x = N/8$, ($N = 1$–7) were prepared by a standard solid-state reaction. Stoichiometric proportions of La_2O_3, $CaCO_3$, and $MnCO_3$ were mixed and heated at 1200 °C for two days with an intermediate grinding. After grinding, the mixture was pressed into pellets and sintered at 1300 °C for 24 h. The phase purity and crystal structure of the samples were characterized by x-ray diffraction (XRD). Figure 1 shows the Ca doping dependence of XRD patterns for LCMO ($x = N/8$, $N = 1$–7) at room temperature; the patterns could be indexed to a *Pnma*-type orthorhombic structure. The EPR spectra were recorded using a Bruker ER200D spectrometer at 9.61 GHz (X band) upon warming within the temperature range 100 K $\leqslant T \leqslant$ 450 K. The measurements were carried out on loose-packed micron-sized crushed crystals.

3. Results

Figures 2(a)–(m) show the EPR spectra recorded as the derivative dP/dH at different temperatures for polycrystalline samples of LCMO with commensurate doping of $x = N/8$, ($N = 1$–7). In the high-temperature paramagnetic region, one broad signal is observed in the EPR spectra for the samples, which was suggested to be a consequence of magnetic

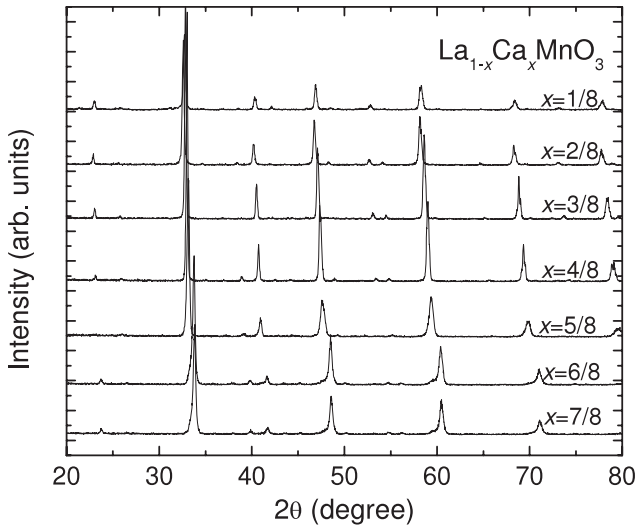

Figure 1. The Ca doping dependence of XRD patterns for polycrystalline samples of $La_{1-x}Ca_xMnO_3$ ($x = N/8$, $N = 1, 2, 3, 4, 5, 6$, and 7) at room temperature.

clusters made of a collection of Mn^{3+} and Mn^{4+} ions [12]. This signal rapidly enhances with decreasing temperature. The lineshape of the signal remains almost symmetric, whereas it becomes distorted approaching magnetic transition temperatures.

In order to precisely determine the EPR parameters, i.e. resonance field (g-factor) and linewidth ΔH, we have fitted the signals with the following equation [13],

$$\frac{\mathrm{d}P}{\mathrm{d}H} \propto \frac{\mathrm{d}}{\mathrm{d}H}\left(\frac{\Delta H}{(H - H_\mathrm{r})^2 + \Delta H^2} + \frac{\Delta H}{(H + H_\mathrm{r})^2 + \Delta H^2}\right), \tag{1}$$

where H_r is the resonance field and ΔH is the linewidth. Illustrations of the fitting results are shown by the solid lines in figure 3, where H_r and ΔH are fitting parameters. As can be seen, the EPR spectra at room temperature can be well described by equation (1) except for samples with $x = 6/8$. The discrepancy between the experimental data and the calculated one occurs below 340 K even though the lineshape of the EPR signal remains symmetric for the sample with $x = 6/8$. As an alternative way to determine the linewidth ΔH at this doping level, the linewidth ΔH can be defined as the half width at half maximum of the absorption line. In practice, one can obtain an equivalent value by calculating the half width between two peaks in the second derivative $\mathrm{d}^2P/\mathrm{d}H^2$ curve.

4. Discussion

Figure 4(a) plots the temperature dependence of the g-values obtained from the resonance condition $h\nu = g\mu_\mathrm{B}H_\mathrm{r}$ for the samples. It is found that the g-values are nearly temperature independent except those close to critical regions. Upon cooling below magnetic transition temperatures, the g-factor rapidly increases, i.e., shifts toward low field, due to the formation of a strong internal field. At the same time, the intensity of the EPR signal dramatically reduces with the disappearance of the PI phase. Interestingly, the g-values divide into two distinct parts for the hole-doped and electron-doped samples. By linearly interpolating the results, we can draw a false colour mapping of the g-factor in the T versus x plane, as shown in figure 4(b). It is

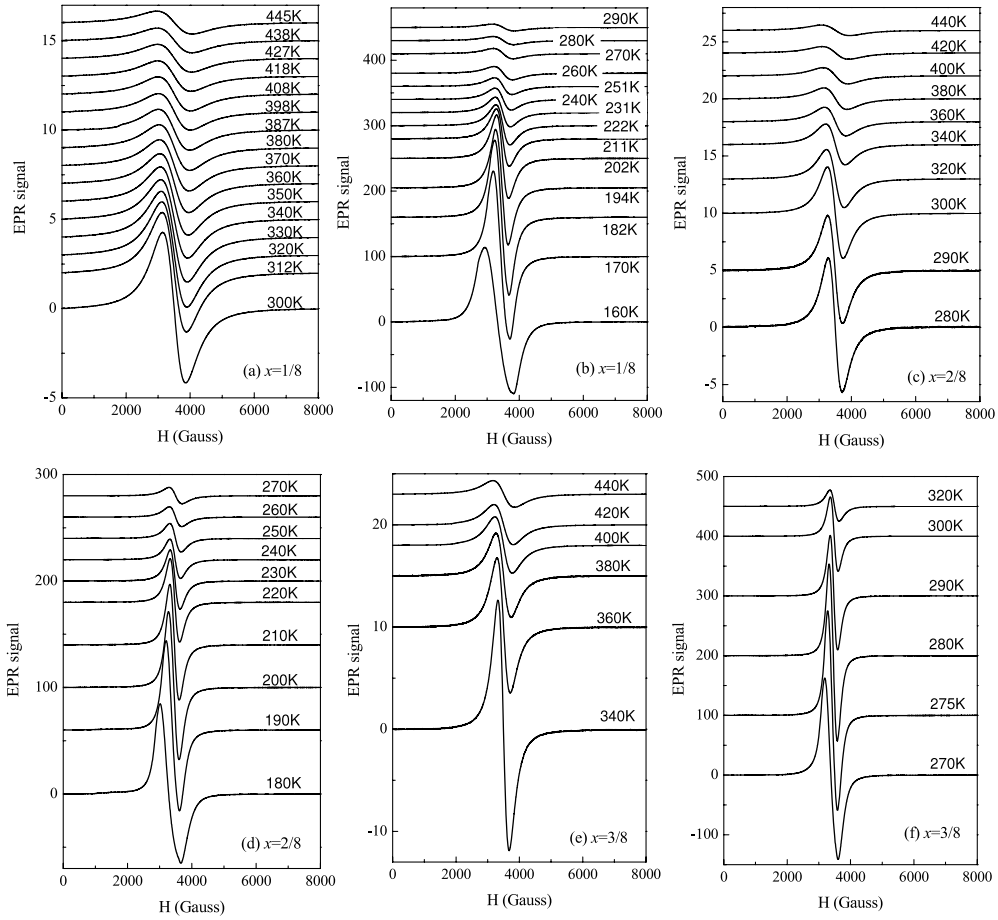

Figure 2. Temperature dependence of EPR spectra of $La_{1-x}Ca_xMnO_3$ at different doping levels: (a), (b) $x = 1/8$, (c), (d) $x = 2/8$, (e), (f) $x = 3/8$, (g), (h) $x = 4/8$, (i), (j) $x = 5/8$, (k) $x = 6/8$, (l), (m) $x = 7/8$. The spectra are shifted for clarity.

noteworthy that the g-factor displays an electron–hole asymmetry forming a phase line centred at $x = 4/8$. Rao *et al* also observed an electron–hole asymmetry feature in the $Pr_{1-x}Ca_xMnO_3$ (PCMO) system, where the g-value for the electron-doped sample ($x = 0.64$) is less than the free electron value $g_e \sim 2.0023$, whereas for the hole-doped one ($x = 0.36$) it is more than g_e at room temperature [14]. Although this variation is very small, Rao *et al*'s [14] and our results suggest that electron–hole asymmetry is a universal feature in the manganites. The mechanism behind this feature is still unknown. We hope that this study will stimulate much more interest on this problem.

Figure 5(a) plots the linewidth ΔH for the samples, which display strong temperature- and doping-dependent behaviours. As a function of T, the EPR linewidth ΔH for all the samples except that with $x = 7/8$ decreases with decreasing temperature. The linewidth ΔH of the sample with $x = 7/8$ saturates rapidly with increasing temperature. Furthermore, it becomes dramatically wide compared with other samples. Upon cooling, ΔH for all samples decreases to a minimum at T_{min}, which is slightly above the ordering temperature. With further decreasing temperature, ΔH increases rapidly. Below the ordering temperature the EPR signals

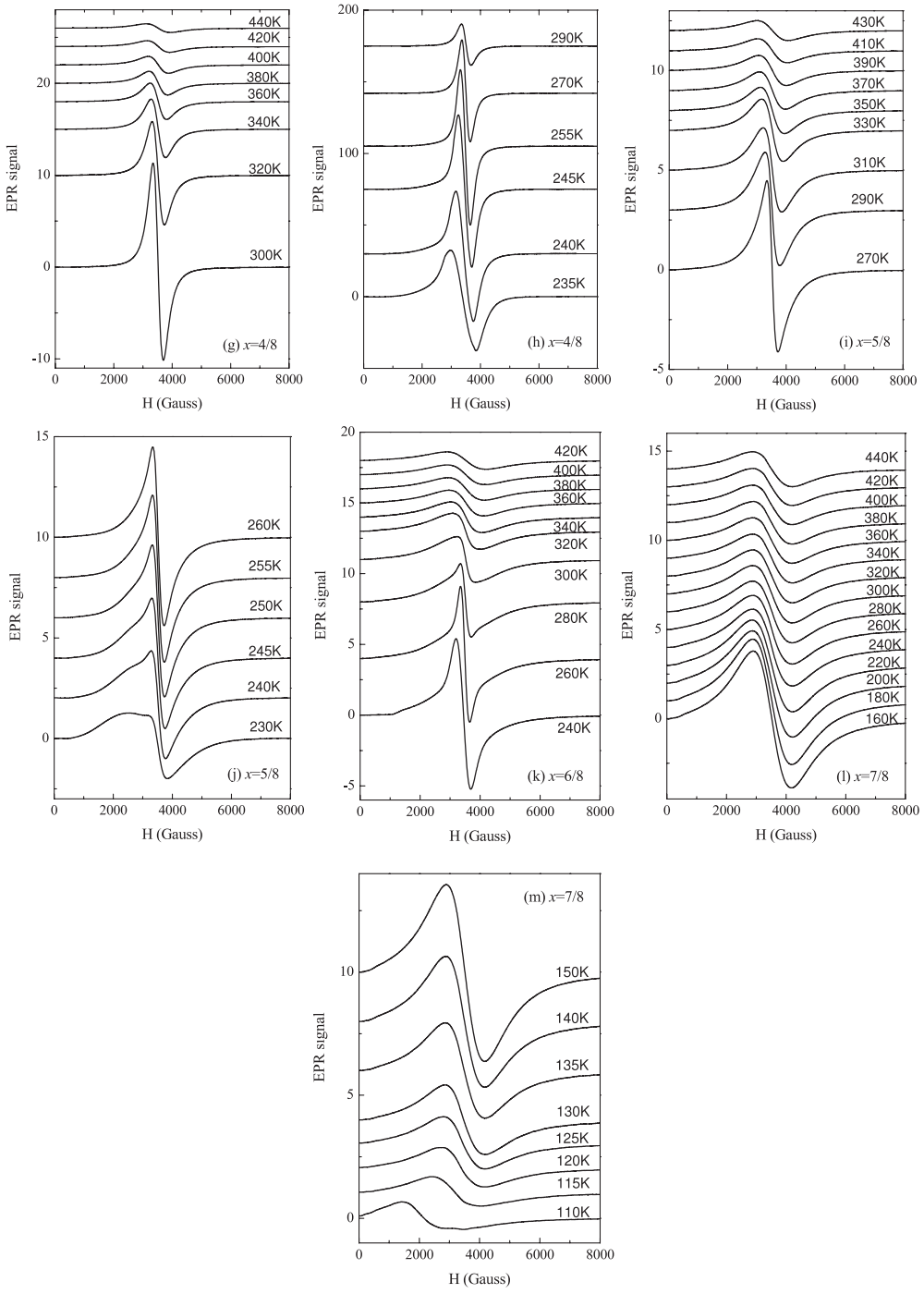

Figure 2. (Continued.)

strongly deviate from a symmetric lineshape. It was reported that the local minimum of ΔH at $T_{\min}$ tends to disappear in perfect single crystals, which results from a two-magnon scattering

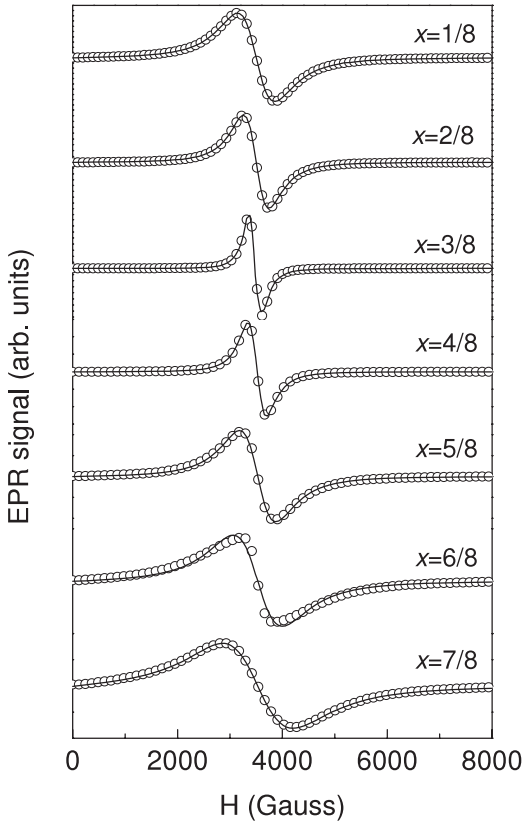

Figure 3. EPR spectra of powder samples of $La_{1-x}Ca_xMnO_3$ ($x = N/8$, $N = 1, 2, 3, 4, 5, 6$, and 7) at 300 K. The solid lines show the fits of the experimental data to equation (1).

relaxation induced by the demagnetization fields of the pores between crystallites [15]. Thus a discussion of the behaviour below T_{min} is meaningless for a powder sample.

We show the mapping of the EPR linewidth in figure 5(b). Remarkably, on approaching the ordering temperatures from above, the narrowing of the EPR linewidth gets strong for $x \leqslant 4/8$, where a colossal magnetoresistance (CMR) effect is observed. It is found that the drop of linewidth ΔH with decreasing temperature in the mapping resembles the contour of the ferromagnetic transition curve in the LCMO phase diagram. The linewidth ΔH as a function of x gets narrowest at $x = 3/8$ at the same temperature (see also figure 3), corresponding to the highest T_C at this doping level. Let us turn to the resistivity ρ at 300 K for LCMO [1]. It shows a slow variation with increasing x from 0 to 1, and no anomalies are observed. It was found, however, that the doping dependence of magnetic susceptibility χ at 300 K displays a strikingly sharp peak at the $x = 3/8$ composition [10]. According to Zener's DE mechanism [2], e_g electrons hop between Mn^{3+} and Mn^{4+} ions while keeping their spin directions due to a strong Hund coupling energy because such hopping is most probable when the spins of t_{2g} electrons of the Mn^{3+} are aligned with those of the adjacent Mn^{4+}. Thus, the enhancement of FM correlation is related to the strongest exchange interactions at $x = 3/8$. The narrowest linewidth ΔH at $x = 3/8$ is associated with an enhanced effectiveness of the DE relative to superexchange interaction in producing an exchange narrowed linewidth [16]. For $x = 7/8$ only a few Mn^{3+} ions are embedded in the lattice, and superexchange interaction

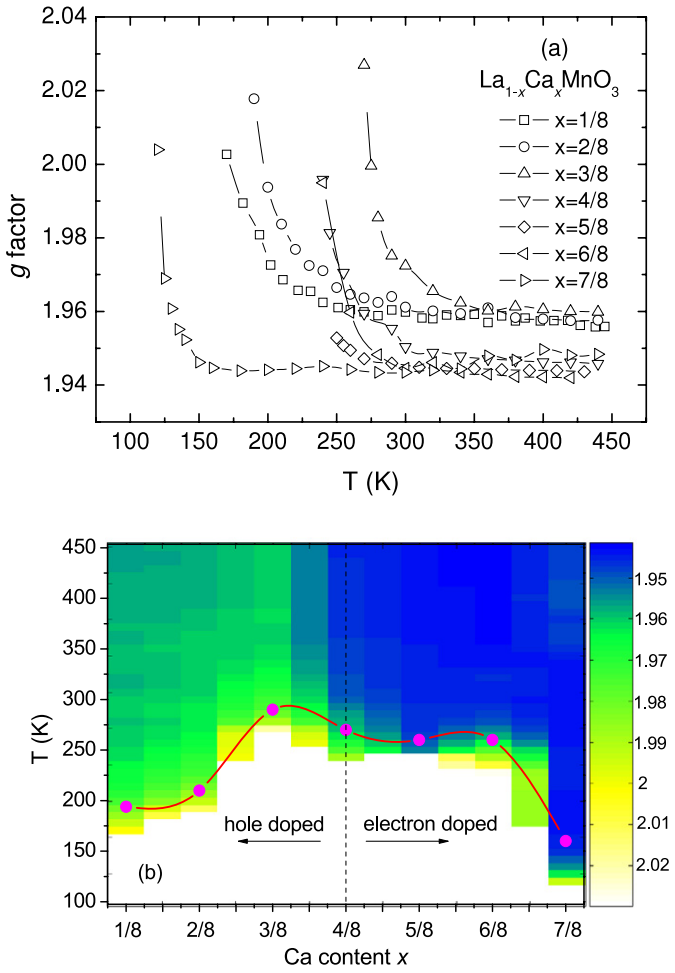

Figure 4. (a) Temperature dependence of the resonance field (H_r) of EPR signals presenting by g-factor for $La_{1-x}Ca_xMnO_3$ samples ($x = N/8$, $N = 1, 2, 3, 4, 5, 6$, and 7). (b) A false colour mapping of the g-factor in the T versus x plane for $La_{1-x}Ca_xMnO_3$. The value of the g-factor at different temperatures and doping levels is given by a false colour scale. The increase of g-factor is shown by the colour bar changing from blue to yellow, which changes from thick grey to white in the print black and white version. The solid magenta circles show T_{min} for the measured compositions, and the red line is a guide to the eye. The dashed line indicates the boundary of two different g-value regimes at $x = 4/8$.

dominates. Thus linewidth ΔH broadens and shows temperature-independent behaviour with the weakening of DE interaction at this doping level. It has been found that the polaronic state near the optimal doping is intrinsically inhomogeneous, consisting of magnetic clusters 10–20 Å in diameter [6–10]. Generally, the polaronic state is a consequence of the strong electron–phonon coupling, enhanced by the JT activity of Mn^{3+} ions in the manganites. On the other hand, the exchange correlation is strongly enhanced for x near 3/8, which is relevant for the presence of short-range polaron correlations. Our observation naturally suggests that the exchange correlation provides the 'glue' for the formation of FM coupled polarons.

Two distinct models in the literature, i.e. spin relaxation and thermally activated small polaron, have been suggested to describe the relaxation mechanism for the temperature

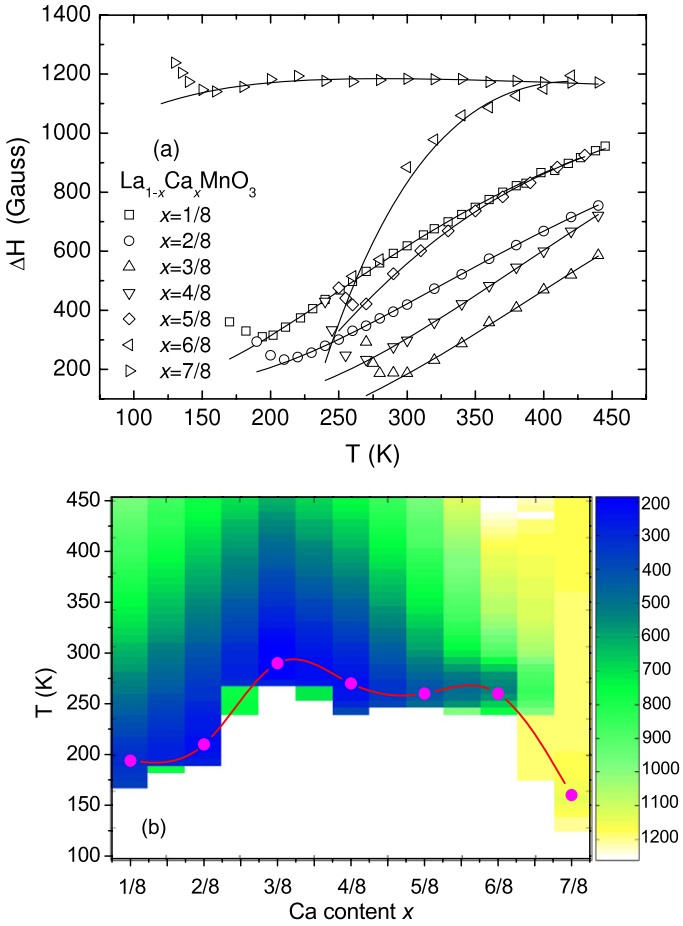

Figure 5. (a) Temperature dependence of the linewidth ΔH for $La_{1-x}Ca_xMnO_3$ samples ($x = N/8$, $N = 1, 2, 3, 4, 5, 6,$ and 7). The solid lines correspond to the best fits of equation (2). (b) A false colour mapping of linewidth ΔH in the T versus x plane for $La_{1-x}Ca_xMnO_3$. The value of linewidth ΔH at different temperatures and doping levels is given by a false colour scale. The drop of linewidth is shown by the colour bar changing from yellow to blue, which changes from white to thick grey in the print black and white version. The solid magenta circles show T_{min} for the measured compositions, and the red line is a guide to the eye.

dependence of the linewidth ΔH in the manganites. The linewidth ΔH shows a linear T dependence in the range $1.1T_C < T < 2T_C$ for hole-doped manganites, which was interpreted in terms of a single-phonon spin–lattice relaxation mechanism [17]. By substituting ^{16}O for ^{18}O, the characteristic differences observed in EPR intensity and linewidth for the two isotope samples were suggested to be caused by a bottlenecked spin relaxation taking place from the exchange-coupled constituent Mn^{4+} ions via the Mn^{3+} Jahn–Teller ions to the lattice [18]. Furthermore, Shengelaya *et al* [19] found that the temperature dependence of the linewidth ΔH can be described by the adiabatic hopping of small polarons, i.e., $\sigma \propto T^{-1} \exp(-E_a/k_BT)$, which is consistent with the existence of a bottleneck EPR regime in the manganites. We have fitted our data shown in figure 5(a) by the following expression:

$$\Delta H = \Delta H_0 + \frac{A}{T} \exp(-E_a/k_BT), \tag{2}$$

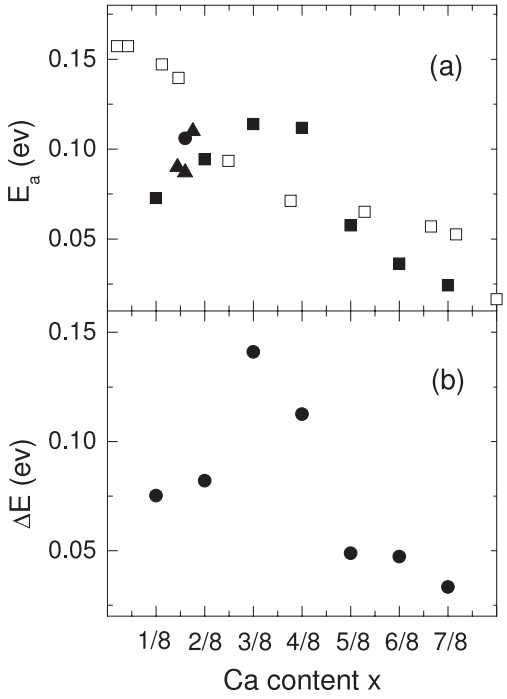

Figure 6. (a) Doping behaviour of the activation energy E_a extracted from the temperature-dependent EPR linewidth and resistivity for the $La_{1-x}Ca_xMnO_3$ system using the adiabatic small-polaron model (equation (2)). The solid circle corresponds to the data at $x = 0.2$ obtained by Shengelaya *et al* [19]. Solid triangles correspond to the data at $x = 0.18$, 0.2, and 0.22 reproduced from [20]. The data obtained by electronic measurements are adapted from [21]. (b) Activation energy ΔE obtained by the fits of double integrated intensity of the EPR signal with the Arrhenius law (equation (3)).

where E_a is the activation energy, i.e., the potential barrier that the polaron must surmount in order to hop into the next site. The E_a values obtained by fitting equation (2) are plotted in figure 6(a). The data obtained in the previous work at $x = 0.18$, 0.2, and 0.22 are also presented in figure 6(a) [19, 20]. It is found that the E_a values display a peak at $x = 3/8$. However, E_a values deduced from the conductivity measurements show a striking divergence from those measured by the EPR technique. As shown in figure 6(a), they decrease smoothly with increasing x [21]. No anomalous behaviours are observed at $x = 3/8$. As can be seen in figure 6(a), the coincidence of E_a values only occurs around $x = 1/3$ and $5/8$. On the other hand, Atsarkin *et al* [22] have measured the longitudinal spin-relaxation time T_1 in the paramagnetic state of three LCMO samples ($x = 0.2$, 0.25, and 0.33). The reported T_1 behaviour contradicts that predicted by the polaron model.

In contrast to the view by Oseroff *et al* [12], Shengelaya *et al* [18] suggested that the EPR signal observed in LCMO is due primarily to Mn^{4+} ions. It was found however, that both Mn^{4+} and Mn^{3+} ions take part in producing the EPR signal. The EPR susceptibility χ_{epr}, deduced from the relation $I \propto \chi_{epr}$ (I is the EPR intensity), could be identified with the magnetic susceptibility χ_{dc}, which supports the suggestion that all the Mn ions contribute to the observed EPR spectra in the whole PI range [23]. In this study, the EPR intensity I was determined by numerical double integration of the measured spectra. Instead of a simple Curie–Weiss law, the

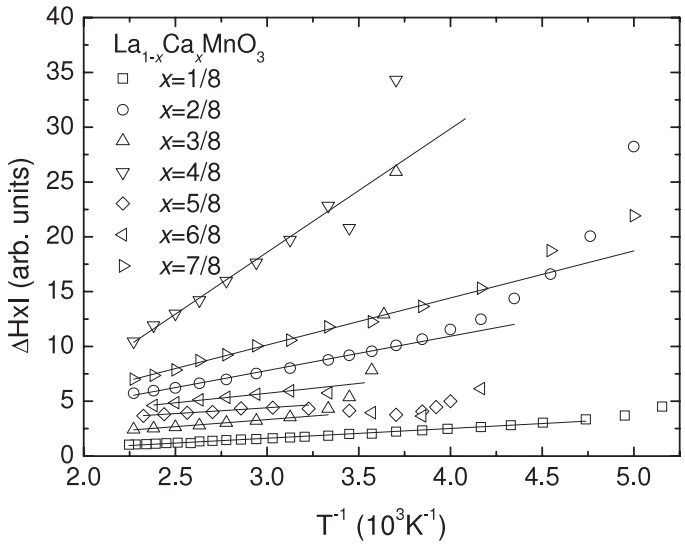

Figure 7. The plots of $\Delta H \times I$ versus $1000/T$ showing a linear behaviour in the whole doping range.

intensity I during the PI regime can be described by a thermally activated model [9, 12, 23],

$$I = I_0 \exp(\Delta E / k_B T), \tag{3}$$

where ΔE is the activation energy. Figure 6(b) shows ΔE obtained by a linear fit of $\ln I$ versus $1000/T$ plots. Interestingly, the activation energy ΔE resembles the result obtained by fitting the linewidth ΔH with equation (2), and peaks at $x = 3/8$. This feature was also observed by Oseroff *et al* [12].

We have demonstrated that the temperature dependence of the linewidth ΔH cannot be ascribed to the mechanism of small-polaron hopping in the whole doping range. According to the theoretical and experimental approaches by Causa and co-workers [23–25], the EPR linewidth in a wide variety of the perovskite manganites is determined by spin–spin (exchange) interactions between the Mn^{3+} and Mn^{4+} ions and so is unrelated to any spin–lattice processes. In all cases studied, the linewidth ΔH away from magnetic and structural transitions can be fitted to a simple expression [23–25],

$$\Delta H = [C/T\chi_{dc}(T)]\Delta H(\infty), \tag{4}$$

where $\Delta H(\infty)$ is a system-dependent constant, and may be identified with the high-temperature limit of the linewidth. Using the relation $I \propto \chi_{epr} \sim \chi_{dc}$, one can easily deduce that the product of $\Delta H \times I$ is in proportion to the inverse temperature. Figure 7 shows the plots of $\Delta H \times I$ versus $1000/T$ above the critical regime. A linear behaviour is clearly observed, as predicted by equation (4). The result is in good agreement with a spin-only relaxation mechanism.

Recently, Huber *et al* pointed out that the spin relaxation mechanism and thermally activated model are equivalent in $La_{0.8}Ca_{0.2}MnO_3$ and $La_{0.67}Sr_{0.33}MnO_3$ [26]. They demonstrated that the similar activation energy observed in figure 6(a) in LCMO for $x \sim 0.2$–0.3 is associated with the static susceptibility containing a thermal activation component. Indirect evidence is that the intensity I of the EPR signals, which is identical with the static susceptibility, follows the thermally activated model, i.e. equation (3). But how do we explain

that the activation energy ΔE obtained by fitting the intensity I to an Arrhenius law displays a sharp peak at $x = 3/8$? The peaking behaviour of ΔE is believed to be related to the strong FM coupling at $x = 3/8$ [10]. It is known that the core spins and the spins of the e_g polarons are aligned parallel due to the Hund's rule correlations, while adjacent Mn^{3+} and Mn^{4+} ions are FM coupled due to the DE interaction in the manganites. When considering that this spin alignment is disrupted by the random hopping of the polarons [26], the large potential barrier, corresponding to the large activation energy, should be overcome in the hopping process due to strong DE interaction at $x = 3/8$. The results suggest that the PI regime in the LCMO phase diagram is more complicated than one's intuition would think, and more detailed research should be done on the role of e_g electron hopping in the whole doping range.

5. Conclusions

In summary, we have demonstrated that the mapping of EPR parameters offers a powerful tool to investigate the high-temperature spin dynamics in the phase diagram of CMR manganites. An electron–hole asymmetry can be clearly observed in the mapping of the g-factor and linewidth ΔH. The narrowing behaviour of the linewidth ΔH as a function of x reveal strong FM coupling at $x = 3/8$. The intensity I follows the thermal activation model, and the activation energy ΔE peaks at $x = 3/8$. The analysis of the linewidth ΔH supports the suggestion that the EPR signal is dominated by spin–spin exchange interaction.

Acknowledgments

This work was supported by the National Nature Science Foundation of China and China Postdoctoral Science Foundation. We would like to thank D L Huber for providing his latest paper on EPR investigation in the manganites.

References

[1] Schiffer P, Ramirez A P, Bao W and Cheong S W 1995 *Phys. Rev. Lett.* **75** 3336
Cheong S W and Hwang H Y 2000 *Colossal Magnetoresistive Oxides* ed Y Tokura (New York: Gordon and Breach Science)
[2] Zener C 1951 *Phys. Rev.* **82** 403
[3] Millis A J, Littlewood P B and Shraiman B I 1995 *Phys. Rev. Lett.* **74** 5144
Millis A J, Shraiman B I and Mueller R 1996 *Phys. Rev. Lett.* **77** 175
[4] Popović Z and Satpathy S 2002 *Phys. Rev. Lett.* **88** 197201
[5] Salamon M B and Jaime M 2001 *Rev. Mod. Phys.* **73** 583
[6] De Teresa J M, Ibarra M R, Algarabel P A, Ritter C, Marquina C, Blasco J, García J, del Moral A and Arnold Z 1997 *Nature* **386** 256
[7] Vasiliu-Doloc L, Rosenkranz S, Osborn R, Sinha S K, Lynn J W, Mesot J, Seeck O H, Preosti G, Fedro A J and Mitchell J F 1999 *Phys. Rev. Lett.* **83** 4393
[8] Adams C P, Lynn J W, Mukovskii Y M, Arsenov A A and Shulyatev D A 2000 *Phys. Rev. Lett.* **85** 3954
[9] Yi H, Hur N H and Yu J 2000 *Phys. Rev.* B **61** 9501
[10] Kim K H, Uehara M and Cheong S W 2000 *Phys. Rev.* B **62** R11945
[11] Wollan E O and Koehler W C 1955 *Phys. Rev.* **100** 545
Goodenough J B 1955 *Phys. Rev.* **100** 564
[12] Oseroff S B, Torikachvili M, Singley J, Ali S, Cheong S W and Schultz S 1996 *Phys. Rev.* B **53** 6521
[13] Ivanshin V A, Deisenhofer J, Krug von Nidda H A, Loidl A, Mukhin A A, Balbashov A M and Eremin M V 2000 *Phys. Rev.* B **61** 6213
[14] Joshi J P, Sarathy K V, Sood A K, Bhat S V and Rao C N R 2004 *J. Phys.: Condens. Matter* **16** 2869
[15] Rivadulla F, López-Quintela M A, Hueso L E, Rivas J, Causa M T, Ramos C, Sánchez R D and Tovar M 1999 *Phys. Rev.* B **60** 11922

[16] Huber D L 1998 *J. Appl. Phys.* **83** 6949
[17] Rettori C, Rao D, Singley J, Kidwell D, Oseroff S B, Causa M T, Neumeier J J, McClellan K J, Cheong S W and Schultz S 1997 *Phys. Rev.* B **55** 3083
[18] Shengelaya A, Zhao G M, Keller H and Müller K A 1996 *Phys. Rev. Lett.* **77** 5296
[19] Shengelaya A, Zhao G M, Keller H, Müller K A and Kochelaev B I 2000 *Phys. Rev.* B **61** 5888
[20] Shames A I, Rozenberg E, Gorodetsky G and Mukovskii Ya M 2003 *Phys. Rev.* B **68** 174402
[21] Worledge D C, Miéville L and Geballe T H 1998 *Phys. Rev.* B **57** 15267
[22] Atsarkin V A, Demidov V V, Vasneva G A and Conder K 2001 *Phys. Rev.* B **63** 092405
[23] Causa M T, Tovar M, Caneiro A, Prado F, Ibañez G, Ramos C A, Butera A, Alascio B, Obradors X, Piñol S, Rivadulla F, Vázquez-Vázquez C, López-Quintela M A, Rivas J, Tokura Y and Oseroff S B 1998 *Phys. Rev.* B **58** 3233
[24] Huber D L, Alejandro G, Caneiro A, Causa M T, Prado F, Tovar M and Oseroff S B 1999 *Phys. Rev.* B **60** 12155
[25] Tovar M, Alejandro G, Butera A, Caneiro A, Causa M T, Prado F and Sánchez R D 1999 *Phys. Rev.* B **60** 10199
[26] Huber D L, Laura-Ccahuana D, Tovar M and Causa M T 2007 *J. Magn. Magn. Mater.* **310** e604